

FINITE ELEMENT ANALYSIS OF THE LATERAL CAPACITY OF COLD-FORMED STEEL SHEAR WALLS AFTER FIRE EXPOSURE

Shuna Ni¹, Xia Yan², Matthew Hoehler³, Thomas Gernay⁴

ABSTRACT

Cold-formed-steel construction frequently relies on strap-braced, cold-formed-steel framed walls as the lateral-force resisting system. While the behavior of these walls has been studied during fire and under lateral loading separately, the influence of multi-hazard interactions – and particularly the effect of fire damage on walls' subsequent lateral load resistance – remains poorly understood. This paper presents a simulation procedure to analyze the thermal and structural response of cold-formed-steel walls when subjected sequentially to fire and lateral load, which is validated against full-scale experiments. The results indicate that the numerical model can capture the post-fire response of cold-formed steel walls, including lateral strength, stiffness, and ductile failure. The lateral behavior of the walls was found to depend primarily on the maximum temperature reached in the cold-formed steel members, and their resulting residual material properties. Then, the validated simulation procedure was used to estimate the residual lateral performance of a strap-braced wall after exposure to various high temperatures. For the residual strength of the cold-formed steel material, data collected from the literature was combined with new test data from the authors to study the effect of variability in material post-fire strength on the wall's response. The outcomes of this research will help engineers to determine the post-fire performance of a wall as a function of the severity of the fire event.

Keywords: Shear walls; Cold-formed steel; Fire; Strap bracing; Lateral resistance; Numerical modelling.

1 INTRODUCTION

Numerous studies have been conducted on the performance of cold-formed steel shear walls under lateral loads caused by earthquakes or wind [1,2,11,12,3–10], axial (gravity) loading from upper stories [13–15], and combinations of axial and lateral loading [9,16]. Walls' sheathing, whether structural panels or non-structural gypsum, plays a role in their strength and stiffness, as well as in restraining torsional modes [9]. Properly designed strap-braced cold-formed steel walls typically fail due to rupture of the strap in tension. The fire performance of cold-formed steel walls has also been investigated, through both experimental and numerical studies [17–22]. Numerical simulation methods and analytical models have been proposed to capture the thermal (fire) response of these walls [19,23], and their results imply that the fire performance of cold-formed steel walls is heavily dependent on the response of the lining protective material (often, gypsum board). The temperature distribution in the walls' framing members is influenced not only by the integrity of the lining throughout a fire, but also by the lining material's thermal properties. Despite the reasonably good understanding of load-bearing walls' behaviour under lateral loads and during (or shortly after) fires, there is a clear need for better understanding of the response under combined action of these

¹ Assistant Professor, Utah State University,
e-mail: shuna.ni@usu.edu, ORCID: <https://orcid.org/0000-0002-8795-176X>

² Graduate Research Assistant, Johns Hopkins University
e-mail: xyan18@jhu.edu, ORCID: <https://orcid.org/0000-0002-1263-3417>

³ Research Structural Engineer, National Institute of Standards and Technologies
e-mail: matthew.hoehler@nist.gov, ORCID: <https://orcid.org/0000-0002-6049-7560>

⁴ Assistant Professor, Johns Hopkins University
e-mail: tgernay@jhu.edu, , ORCID: <https://orcid.org/0000-0002-3511-9226>

hazards [1]. Accurately ascertaining the lateral-force resisting capacity of cold-formed steel walls after exposure to fire is important for several reasons. First, after a fire that leaves a structure relatively undamaged, an engineer needs to assess the residual capacity of the system to inform repair or replacement decisions. For a relatively mild fire, replacement of the compartment lining material (e.g., gypsum) may suffice to rehabilitate the structure, but the possible reduction in capacity due to the thermal exposure nevertheless needs to be quantified. Another situation where knowledge of multi-hazard behaviour can be critical is fires on windy days, which are common in wildland-urban interface (WUI) communities [24]. Finally, a reduction in lateral capacity due to fire may imperil a structure's stability during post-fire earthquake response, e.g., in a situation where an earthquake triggers a fire [25], which in turn is followed by aftershocks.

Therefore, this research focuses on the residual lateral performance of cold-formed steel strap-braced walls after fire exposure, with the aim of advancing understanding of the response to cascading hazards and informing post-fire repairs. In Section 2, a simulation procedure was developed and validated for the post-fire lateral performance of cold-formed steel shear walls. In Section 3, collected test data on the post-fire residual properties of cold-formed steel were discussed, focusing primarily on residual strength. Because numerical simulations based on the finite element method are time-consuming, they are not convenient for most day-to-day applications. Section 4 describes how the validated simulation procedure can be used to determine the residual lateral performance of cold-formed steel shear walls after exposure to various high temperatures; these numerical data can then be used by engineers to quickly estimate the residual wall capacity based on the fire severity.

2 SIMULATION PROCEDURE AND VALIDATION AGAINST NIST TESTS

A finite element model is developed in SAFIR [26] to analyze the thermal and mechanical response of cold-formed steel strap-braced walls when subjected sequentially to fire followed by lateral deformation. Each step of the proposed numerical modelling strategy (i.e., heat transfer analysis and mechanical analysis) is validated against full-scale experimental test data from the National Institute of Standards and Technology (NIST) [1]. The objective of these tests was to investigate the influence of fire on the lateral performance of cold-formed steel shear walls [1,27].

2.1 Heat transfer analysis

The heat transfer across the section of a cold-formed steel wall was modelled using nonlinear finite element analysis with the software SAFIR [26]. A 2D thermal analysis of a cross section was conducted using solid conductive elements. Convective and radiative heat transfer was considered at the boundaries on each side of a wall. In addition, radiative and convective heat transfer was considered in cavities. The integration in time of the thermal equilibrium equation is done implicitly, using the implicit single step scheme of the generalized central point. The objective of the thermal analysis is to verify the ability of the finite element model to capture the physics of heat transfer in a wall specimen using conductive elements for the gypsum and steel and capturing the heat transfer in cavities. As the thermal model assumes a constant geometry of a structural system, it cannot capture the disintegration of gypsum boards which may occur in experiments and result in direct fire exposure of steel studs.

The thermal properties of the materials are considered as temperature dependent. The properties of steel follow the model from Eurocode 3 EN1993-1-2 [28]. The gypsum boards used in the tests were a Type X. Since the thermal properties are not reported in [1], the temperature-dependent properties of the gypsum in the thermal analysis are taken in accordance with the recommendations by Keerthan and Mahendran [29] based on their study of similar Type X gypsum boards under standard fire exposure. The density of gypsum board is assumed as 700 kg/m².

The wall from Test S03 in the NIST campaign, for which the gypsum boards exhibited a relatively good integrity throughout the experiment, was selected for the numerical modelling. The 2D cross section (as shown in Figure 1) that represents the section at the top third of the wall was modelled for the heat transfer analysis, with the thermal boundary condition of the fire-exposed side defined by temperatures measured by the top three plate thermocouples. The software SAFIR computes the heat flux \dot{q} at the boundary using

equation (1). At the unexposed sides of the wall, heat loss by convection and radiation toward the environment at ambient temperature (assumed to be 20 °C) is captured. Heat transfer in the cavities of the wall is also considered.

$$\dot{q} = h(T_g - T_s) + \sigma \epsilon (T_g^4 - T_s^4) \quad (1)$$

where

T_g is the measured adiabatic temperature at the boundary

h is the coefficient of convection (35 kW/m² for the hot surface and 4 kW/m² for the cold surface)

σ is the Stefan-Boltzmann constant, and ϵ is the emissivity of the material (0.9 for gypsum and 0.7 for steel)

T_s is the temperature of the surface of the solid at the boundary

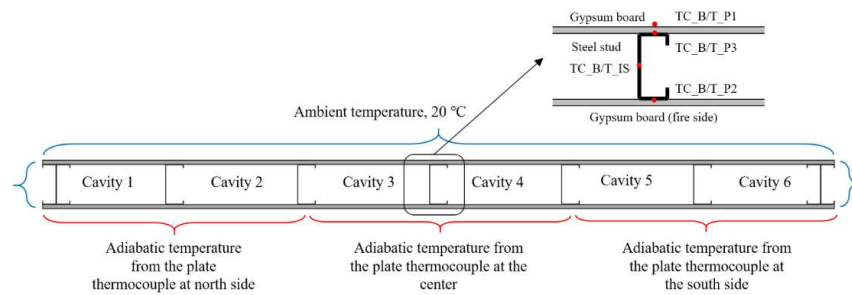


Figure 1. Sketch of the wall cross section and thermal boundary conditions for the wall in Test S03.

Figure 2 shows the temperature distribution in the top part of the wall cross-section after 15 min of fire exposure. Thermal gradients develop in the steel stud as a result of the one-side fire exposure. Figure 3 shows the comparison of the experimental and numerical temperatures. The values are given across the section at the central stud (as shown in Figure 1), at the height of 46 cm from the top of the wall. The temperature values below the measurement points in Figure 3 are the difference in maximum temperature between the experimental measurements and the numerical model. The numerical maximum temperature reasonably agrees with the measured maximum temperature, with the difference in maximum temperature ranging between 39 °C (TC-T-P1) and 7 °C (TC-T-IS). The initial ramp-up of temperature up to 100 °C is not well captured. While the measured temperatures show a fast ramp-up followed by a plateau at 100 °C, the numerical model predicts a more gradual behaviour; yet the numerical model catches up to the experimental values at 100 °C and reasonably follows the trends thereafter. Overall, the numerical model captures the different phases of temperature increase, peak value, and temperature decrease.

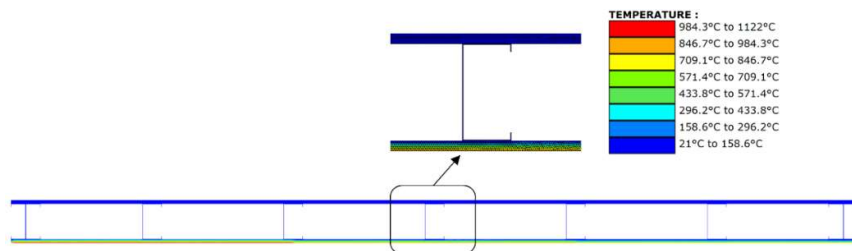


Figure 2. Temperature distribution in the wall cross section at the top part after 15 min of fire exposure.

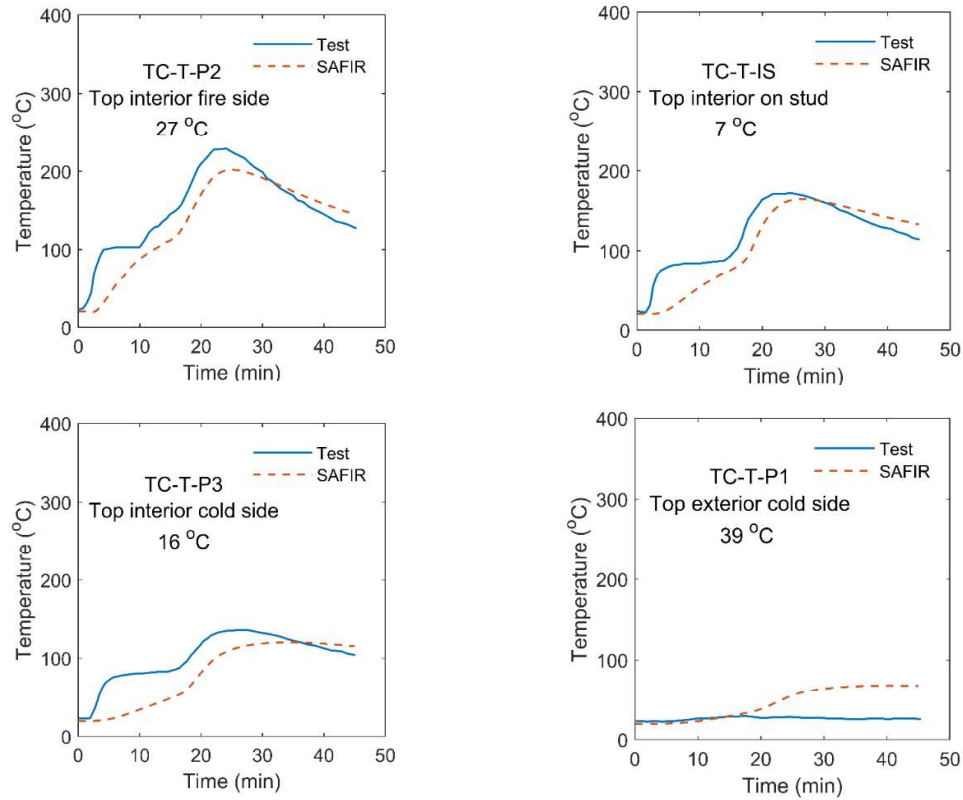


Figure 3. Evolution of temperature in the central stud section at 46 cm from the top of the wall. (Temperature values noted on the plots are the difference in maximum temperature between the experimental measurement and the numerical model).

2.2 Mechanical analysis

Following the thermal analysis to determine the temperature distribution in the wall, a mechanical analysis is performed to evaluate the mechanical response. The numerical model was built to capture the post-fire response of the wall under lateral loading. Previous studies, for example by Chen [22], have shown that the critical temperature at failure for a cold-formed steel wall mainly depends on the maximum temperature a wall has been exposed to. Herein, the effects of the fire exposure on the wall were captured by considering the degradation of the material properties corresponding to the maximum reached temperature throughout the fire exposure.

Figure 4 shows the mechanical model of a cold-formed steel strap-braced wall in SAFIR. The three-dimensional (3D) mechanical analysis is a geometric and material non-linear analysis using shell finite elements. The SAFIR model includes an entire cold-formed steel wall (Figure 4) but the gypsum boards are omitted since the gypsum boards integrity is usually damaged by the fire and the effect of stud bracing is lost due to temperature degradation [30]. No geometric imperfections, residual stresses, or residual strains were included in the model. In the absence of gypsum boards to restrain the brace, the compressive braces rapidly experienced buckling, thus limiting their contribution to the mechanical response. Therefore, the compression braces were not modelled to facilitate convergence far into the global failure mode.

The stiff (truss) loading beam used in the experiment is modelled using beam finite elements, as shown in Figure 4. The degree of freedom of this beam corresponding to the out-of-plane displacement is blocked. The loading is modelled by applying imposed longitudinal displacements at one extremity of the top track. At the bottom track, at each line of shear bolts, three nodes are blocked for the displacement in the horizontal direction. At the two ends of the bottom track, part of the web of the chord studs is connected to hold-down attached to the ground. In the model, this stiff plate condition was created by linking the degrees of freedom of the nodes of the stud web in the hold-down area together, with the central node of this area serving as the primary node. The central node of the stud web in the hold-down area is connected to the ground using

a spring element with a stiffness of 9.9 kN/mm in tension and 100 times that value in compression, as recommended by Leng et al. for this type of connector [31]. Frame members (e.g., studs and tracks) are assumed to be perfectly tied to each other [32].

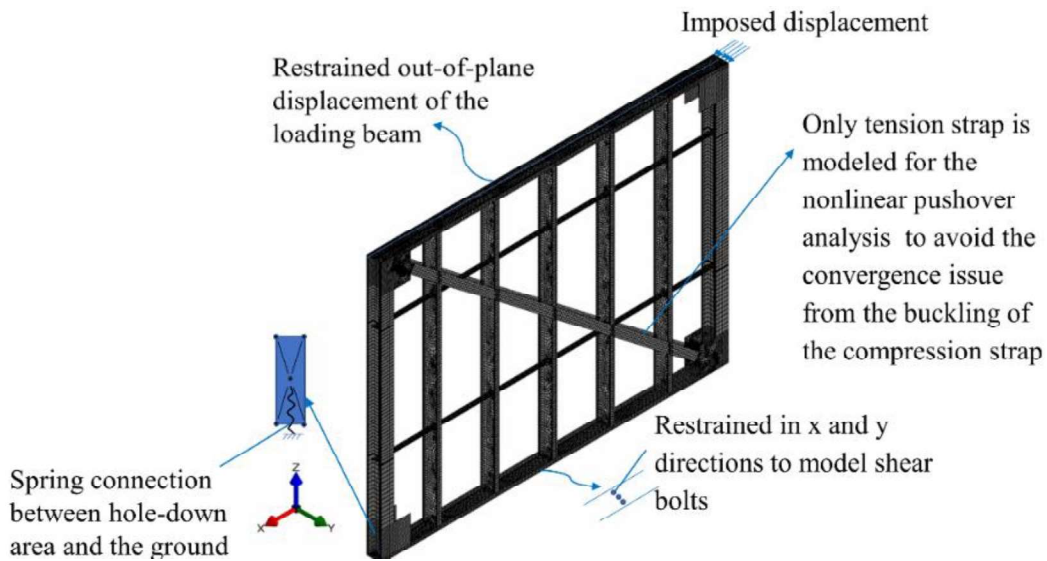


Figure 4. Mechanical model of the cold-formed steel strap-braced wall in SAFIR.

Test S02 in the NIST test campaign was used to validate the simulation method described above. In the test campaign, Test S02 was subjected to cyclic horizontal loading at ambient temperature and after exposure to fire. Figure 5 shows the specimen after the fire test and prior to application of the mechanical loading. The gypsum boards on both sides of the wall had nearly disintegrated due to the fire exposure and there was severe oxidation of the steel strap near the top gusset plate on the south end of the specimen. When the cyclic loading was applied, failure was reached by tension fracture of the straps where the oxidation occurred (top-south) at low load and small displacement levels. However, cycling was continued after this failure. The straps running in the opposite direction had experienced lower temperatures and exhibited unreduced capacity, reduced stiffness, and increased ductility (achieve 10 % story drift ratio) and the testing was terminated when the compression chord associated with the intact strap (north chord) buckled.

The mechanical response of this wall after fire exposure was simulated using nonlinear collapse pushover analysis in the finite element software SAFIR [26]. In the numerical mechanical analysis, the steel model is elastoplastic with a von Mises yield function and isotropic nonlinear hardening (STEELEC32D in SAFIR). The value at ambient temperature of the 2% offset yield strength, ultimate strength, and young's modulus is 390 MPa, 490 MPa and 210 GPa, respectively; the Poisson's ratio is 0.3. Cold-formed steel material collected from the strap bracing used in the NIST experiments was tested at JHU to determine its mechanical properties after exposure to elevated temperatures [33]. The residual mechanical properties were determined from the stress-strain curves and the strength retention factors are summarized in Figure 6. The temperature histories of the wall in Test S02 at different locations are provided in the NIST technical report [1]; the maximum temperatures reached in different parts of the wall are given in Figure 7. From the maximum reached temperature, the residual modulus and yield stress (2% offset) were calculated and were assigned to the shell elements based on the post-fire material tests.



Figure 5. Photograph of the fire exposed side of the wall in Test S02 after the fire test (before cycling) [1].

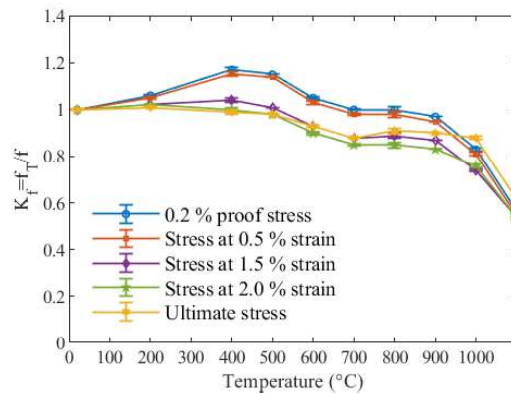


Figure 6. Post-fire retention factors for the strength properties of the tested cold-formed steel.

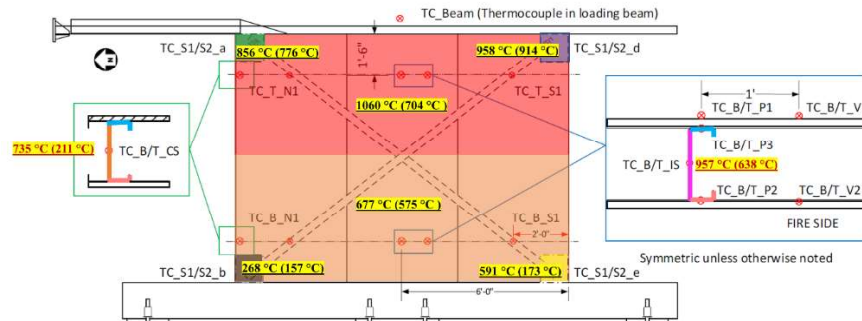


Figure 7. Areas assigned with different material degraded properties [1].

The load-displacement response is plotted in Figure 8. The experimental and numerical responses exhibit a similar behaviour, which is approximately bilinear. The stiffness predicted by the model agrees very well with the experimental stiffness. It is noted that the constitutive steel model, based on Eurocode EN1993-1-2, has a horizontal plateau at the input value of the material strength. Given the large displacements experienced by the wall at failure, strain hardening is expected in the material of the strap bracing. This is supported by examination of the test curve in Figure 8, which exhibits some hardening. Moreover, our test data have shown that as the peak history temperature increases, $k_{2,0}$ decreases at a greater rate than k_u , as shown in Figure 6, which means that fire exposure makes the strain-hardening effect more pronounced for the tested cold-form steel. This would explain why the use of the 2% yield stress with the Eurocode-based law leads to the underestimation of the peak strength of the wall in Test S02. Therefore, the simulation of the wall from Test S02 was repeated using the residual ultimate strength (f_u) instead of the residual 2% yield stress ($f_{2,0}$). The model with f_u captures the upper bound of the capacity that can be developed by the shear wall, see Figure 8.

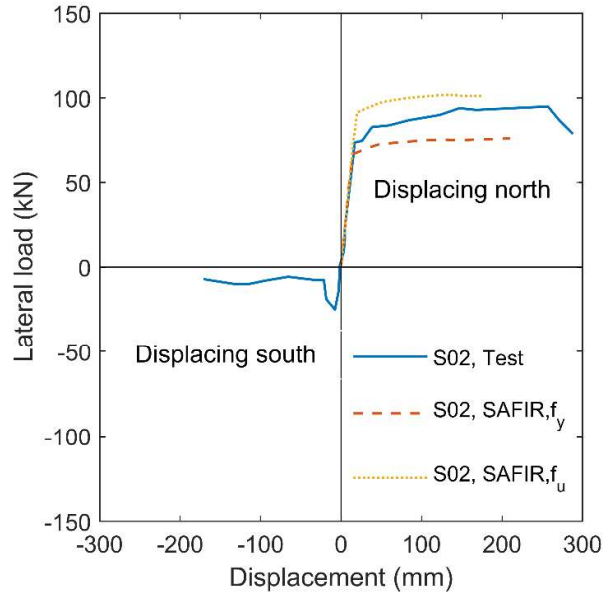
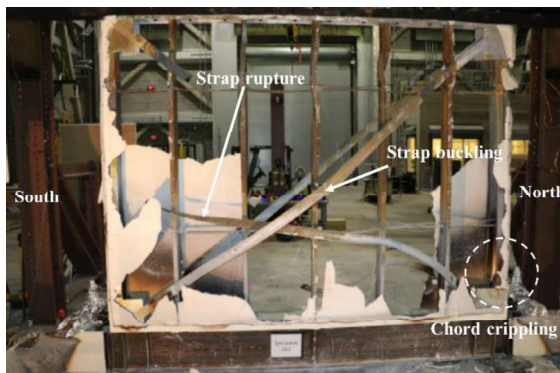
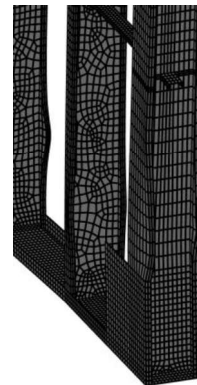


Figure 8. Lateral load versus drift during mechanical loading of steel strap-braced walls

Figure 9a shows a photograph of the specimen after the test. As mentioned previously, the strap running to the top south gusset failed early in the load cycling and no longer participated in the structural response. Crippling of the north chord is apparent when the wall moved northward. Figure 9b also shows the crippling of the chord in compression at the end of the numerical analysis in SAFIR. This local instability occurred after significant yielding of the intact strap (evidenced by the buckling of the elongated strap when the wall was recentred), in accordance to observation during the test [1]. Examination of the distribution of maximum principal strains in the numerical model (as shown in Figure 10) reveals a strain concentration at this location, with a maximum value near the gusset connection of 14.9 %, i.e., about the beginning of the descending branch of the constitutive law. The analysis eventually stopped due to lack of numerical convergence linked to high stress concentrations at the shell element near the bottom track boundary supports that model the shear bolts.



(a) Rupture of the strap in the cyclic-loading test [1]



(b) Crippling of the chord in compression (SAFIR f_y analysis - displaced scale: 1)

Figure 9. Failure mode of the wall loaded after severe fire exposure (Test S02).

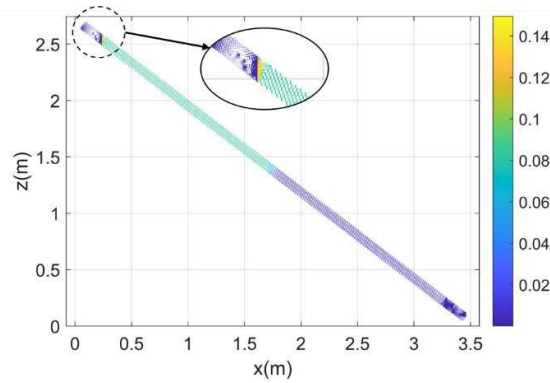


Figure 10. Maximum principal strains in the tensile strap obtained by numerical modelling.

3 TEST DATA FOR RESIDUAL PROPERTIES OF COLD-FORMED STEEL

Figure 11 shows data collected from different sources on the retention factors of the ultimate strength of cold-formed steel. Tests were also conducted by the authors at JHU; the method to obtain residual properties is described in [34]. It can be observed that the post-fire ultimate strength starts to decrease when the temperature is higher than 300 °C, beyond which a fast reduction is observed. After exposure to a temperature higher than 500°C, the reduction in ultimate strength becomes more gradual. Compared with conventional cold-formed steels, high-strength cold-formed steels (yield strength ≥ 460 MPa) tend to show larger reduction in ultimate strength at a given temperature. Significant scatter is observed in the data, which suggests the necessity to consider the upper bound, lower bound, and mean value of the data in the following analysis. The three laws used for the post-fire retention factors of ultimate stress are shown by the solid lines in Figure 11.

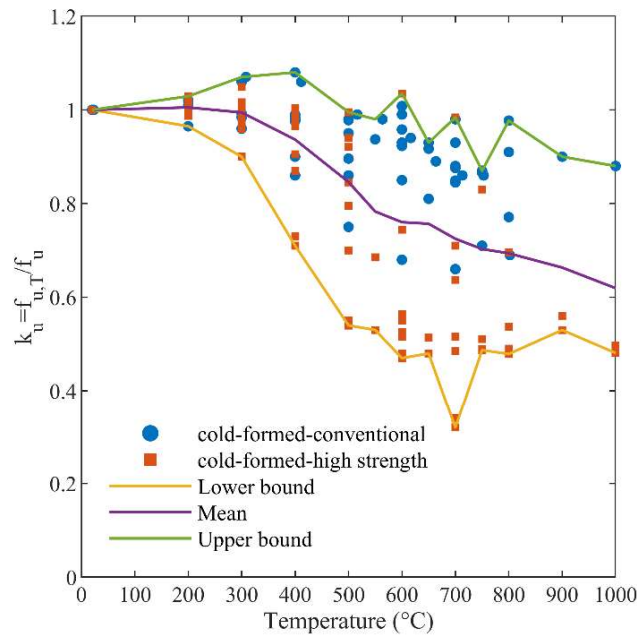


Figure 11. Literature data for post-fire retention factors of cold-formed steel.

4 RESIDUAL PERFORMANCE OF COLD-FORMED STEEL SHEAR WALLS

The experiments and the validated numerical models show that the residual (i.e., post-fire) lateral performance of a strap-braced, cold-formed steel framed wall is governed by the maximum reached temperature of the steel during the fire event and the resulting steel residual properties. Therefore, in this

section, a series of analysis are conducted to study the variation of the residual performance of a wall after exposure to different levels of temperature. The wall tested by NIST and described in Section 2 is used as prototype. Peak steel temperatures of 300 °C, 600 °C and 900 °C are considered. These are chosen to correspond qualitatively to mild, intermediate, and severe fire events, in the meaning of uncontrolled fires that result in steel temperatures lower, about the same, or higher than that considered as the limit in the prescriptive standard fire rating system. Given the observed scatter of residual strength for cold-formed steel (Section 3), the values of the retention factors corresponding to the upper bound, mean value, and lower bound are considered each at the three temperatures. Young's modulus was assumed to regain its initial value after cooling down.

The lateral load versus drift for each scenario is shown in Figure 12. Figure 12a, Figure 12b and Figure 12c are the results based on the lower-bound, mean, and upper-bound material strength retention factors, respectively. The curve for 600 °C is below that for 900 °C in Figure 12a; the curve for ambient temperature is below that for 600 °C in Figure 12c. Both are consistent with the variation of ultimate-strength retention factors with temperatures, as shown in Figure 11. In Figure 12c, the curve for ambient temperature is below the curves for 300 °C, consistent with the increase in ultimate stress observed in the upper bound of retention factors in the range of 100°C ~ 400 °C in Figure 11.

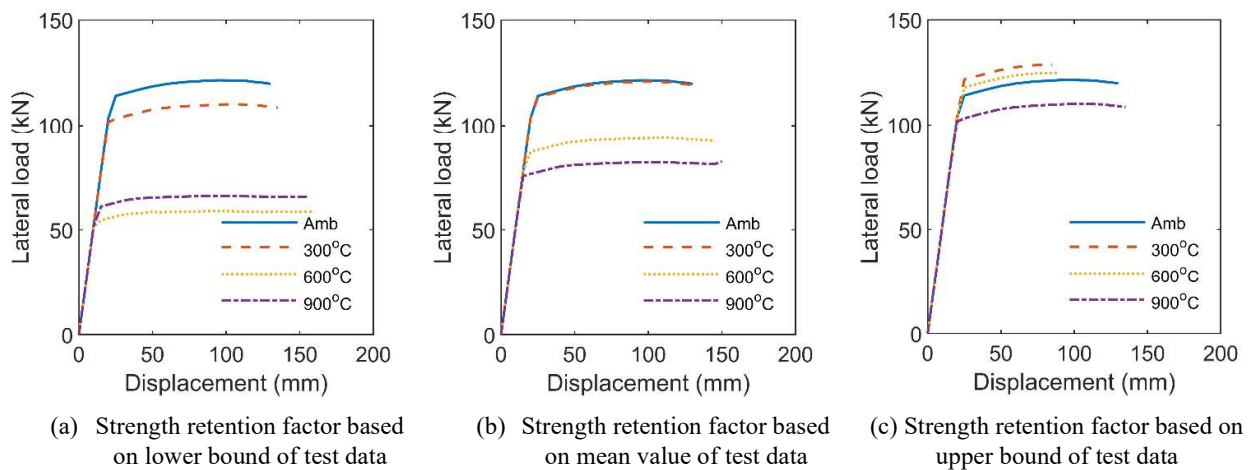


Figure 12. Lateral load versus drift during mechanical loading of steel strap-braced walls after exposure to 300 °C, 600 °C, and 900 °C.

The definition of wall response quantities is shown in Figure 13, including lateral strength (F_{max}), secant stiffness (K) calculated at $0.75F_{max}$, and maximum drift (Δ_{max}). Those wall response quantities of fire-damaged walls were extracted from Figure 14 for comparison to those of the wall without fire damage. The variations of wall response ratios with maximum reached temperatures are summarized in Figure 14. In general, as the temperature increases, the lateral strength of a wall decreases. The strength reduction of the wall ranges from 9% (as shown in the yellow line in Figure 14a) to 46% (as shown in the blue line in Figure 14a) if it is exposed to a maximum reached temperature equal to 900°C. The stiffness of the wall remains approximately constant. This is explained by the fact that Young's modulus of steel is recovered after cooling. Also, the contribution of the nonstructural elements (i.e., gypsum) on the wall's structural response is neglected in the model. In the physical specimen, fire damage to the gypsum would result in a stiffness decrease after the fire. However, the gypsum would be replaced as part of the repairs. The results show that the structural elements would maintain their stiffness after the considered thermal exposure. The variation of maximum drift with temperatures is relatively complex. For the results based on the lower bound of the material strength retention factors, the ductility increases and then begin to decrease at 600 °C; for the results based on the mean value, the ductility increases continuously; for the results based on the upper bound, the ductility decreases first and then increases. Such a complex trend for maximum drift has also been observed in the studies about the post-fire seismic behaviour of reinforced concrete walls [35].

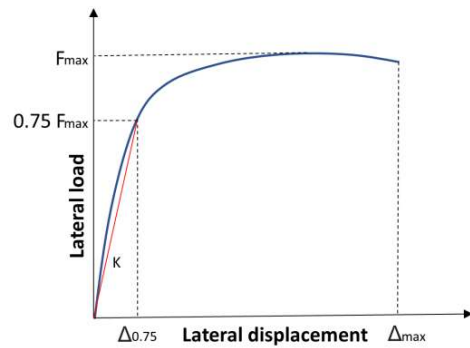


Figure 13 Definition of wall response quantities

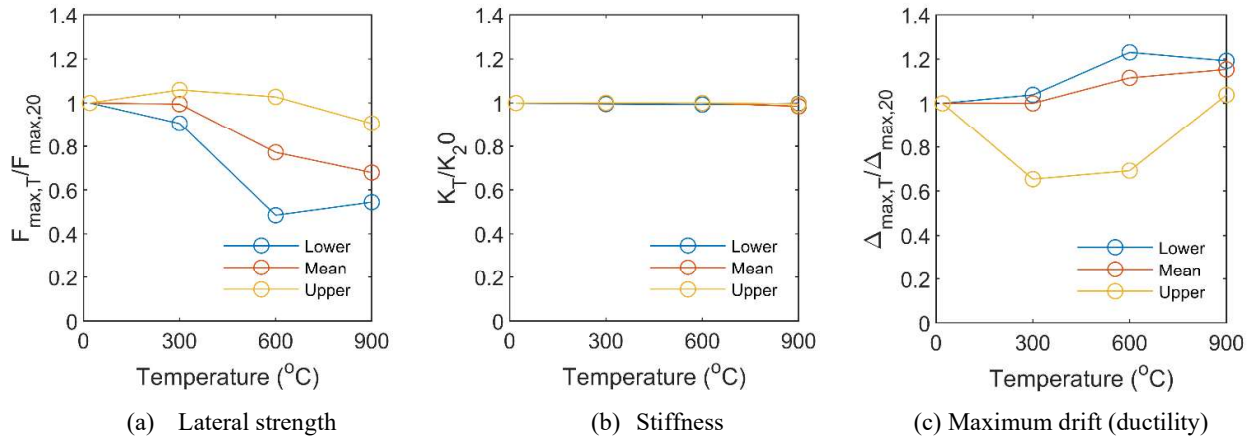


Figure 14. Variation of residual lateral performance of cold-formed steel walls with maximum reached temperatures

5 CONCLUSIONS

A numerical strategy was presented in this paper for modelling and assessing the thermal and post-fire mechanical response of cold-formed steel strap-braced walls. The numerical strategy (both the thermal analysis and mechanical analysis) was validated by the test data provided by the NIST [1]. The thermal analysis can predict the temperature distribution across the section, provided the thermal properties of the gypsum are known, and the integrity of the system is maintained; the mechanical analysis could accurately capture the failure mode, stiffness, and lateral strength of the fire-damaged cold-formed steel wall by modifying the material properties according to the maximum temperatures reached by the wall at different parts. This also suggests that the post-fire lateral resisting capacity of this type of cold-formed steel wall system could be predicted by extending existing analytical methods using the residual mechanical properties for cold-formed steel. The validated numerical strategy was used to estimate the residual lateral performance of the strap-braced walls after exposure to various high temperatures. For the residual strength of the cold-formed steel material, data collected from the literature was combined with new test data from the authors to study the effect of variability in material post-fire strength on the wall's response. The results show that the variations of the wall's response quantities with maximum reached temperature are very different for different response quantities. The trend is relatively consistent for lateral strength and stiffness while it varies significantly for maximum drift when the material ultimate-strength retention factors used in the simulation change from the lower bound of material test data to the upper bound.

In the future, a series of prototypical cold-formed steel walls will be designed, and the variation of their residual wall performance (including lateral-load capacity, lateral stiffness, and ductility or maximum drift) with maximum reached temperatures will be quantified using the validated numerical model. The maximum reached temperatures can also be related to parameters of the validated heat transfer model including fire severity and thermal properties of the gypsum. The outcomes of this research will help engineers to determine the post-fire performance of a wall as a function of the severity of the fire event.

REFERENCES

1. Hoehler, M. S., Andres, B. & Bundy, M. F. Influence of Fire on the Lateral Resistance of Cold-formed Steel Shear Walls – Phase 2: Oriented Strand Board, Strap Braced and Gypsum-Sheet Steel Composite, NIST Technical Note 2038. (2019) doi:10.6028/NIST.TN.2038.
2. Wang, X. et al. Seismic performance of cold-formed steel wall systems in a full-scale building. *J. Struct. Eng.* 141, 04015014 (2015).
3. Peköz, T. Rep. No. CF87-1, Development of a Unified Approach to the Design of Cold-formed Steel Members. <https://books.google.com/books?id=TFeIXwAACAAJ> (1987).
4. Kechidi, S., Macedo, L., Castro, J. M. & Bourahla, N. Seismic risk assessment of cold-formed steel shear wall systems. *J. Constr. Steel Res.* 138, 565–579 (2017).
5. Zeynalian, M. & Ronagh, H. R. Seismic performance of cold formed steel walls sheathed by fibre-cement board panels. *J. Constr. Steel Res.* 107, 1–11 (2015).
6. Gerami, M. & Lotfi, M. Analytical analysis of seismic behavior of cold-formed steel frames with strap brace and sheathings plates. *Adv. Civ. Eng.* 2014, 1–22 (2014).
7. Shahi, R., Lam, N., Gad, E., Wilson, J. & Watson, K. Seismic performance behavior of cold-formed steel wall panels by quasi-static tests and incremental dynamic analyses. *J. Earthq. Eng.* 21, 411–438 (2017).
8. Landolfo, R., Corte, G. D. & Fiorino, L. Testing of sheathed cold-formed steel stud shear walls for seismic performance evaluation. in *13th World Conference on Earthquake Engineering* 2697 (2004).
9. Kechidi, S., Macedo, L., Castro, J. M. & Bourahla, N. Design and assessment of cold-formed steel shear wall systems located in moderate-to-high seismicity regions. *Key Eng. Mater.* 763, 645–652 (2018).
10. Vieira, L. C. M. & Schafer, B. W. Lateral stiffness and strength of sheathing braced cold-formed steel stud walls. *Eng. Struct.* 37, 205–213 (2012).
11. Peterman, K. D. & Schafer, B. W. Sheathed cold-formed steel studs under axial and lateral load. *J. Struct. Eng.* 140, 04014074 (2014).
12. Moen, C. D. & Schafer, B. W. Direct strength method for design of cold-formed steel columns with holes. *J. Struct. Eng.* 137, 559–570 (2011).
13. Green, G. G., Winter, G. & Cuykendall, T. R. *Light Gage Steel Columns in Wall-braced Panels.* (Cornell University, 1947).
14. Tian, Y. S., Wang, J. & Lu, T. J. Axial load capacity of cold-formed steel wall stud with sheathing. *Thin-Walled Struct.* 45, 537–551 (2007).
15. Kechidi, S., Fratamico, D. C., Schafer, B. W., Miguel Castro, J. & Bourahla, N. Simulation of screw connected built-up cold-formed steel back-to-back lipped channels under axial compression. *Eng. Struct.* 206, 110109 (2020).
16. Pham, M. M., Mills, J. E. & Zhuge, Y. Experimental capacity assessment of cold-formed boxed stud and c stud wall systems used in australian residential construction. *J. Struct. Eng.* 132, 631–635 (2006).
17. Gerlich, J. T., Collier, P. C. R. & Buchanan, A. H. Design of light steel-framed walls for fire resistance. *Fire Mater.* 20, 79–96 (1996).
18. Kodur, V. K. R. & Sultan, M. A. Factors influencing fire resistance of load-bearing steel stud walls. *Fire Technol.* 42, 5–26 (2006).
19. Alfawakhiri, F. Behaviour of Cold-formed-steel-framed Walls and Floors in Standard Fire Resistance Tests. (Carleton University, 2002). doi:10.22215/etd/2002-05029.
20. Gunalan, S., Kolarkar, P. & Mahendran, M. Experimental study of load bearing cold-formed steel wall systems under fire conditions. *Thin-Walled Struct.* 65, 72–92 (2013).
21. Gunalan, S. & Mahendran, M. Review of current fire design rules for cold-formed steel wall systems. *J. Fire Sci.* 32, 3–34 (2014).
22. Chen, W., Ye, J., Zhao, Q. & Jiang, J. Full-scale experiments of gypsum-sheathed cavity-insulated cold-formed steel walls under different fire conditions. *J. Constr. Steel Res.* 164, 105809 (2020).
23. Gunalan, S. & Mahendran, M. Finite element modelling of load bearing cold-formed steel wall systems under fire conditions. *Eng. Struct.* 56, 1007–1027 (2013).

24. Encyclopedia of Wildfires and Wildland-Urban Interface (WUI) Fires. (Springer International Publishing, 2020). doi:10.1007/978-3-319-51727-8.
25. Gernay, T. & Khorasani, N. E. Resilience of the built environment to fire and fire-following-earthquake. in Resilient Structures and Infrastructure (eds. Noroozinejad Farsangi, E., Takewaki, I., Yang, T., Astaneh-Asl, A. & P., G.) 417–449 (Springer, 2019). doi:10.1007/978-981-13-7446-3.
26. Franssen, J.-M. & Gernay, T. Modeling structures in fire with SAFIR®: theoretical background and capabilities. *J. Struct. Fire Eng.* 8, 300–323 (2017).
27. Hoehler, M. S. et al. Behavior of steel-sheathed shear walls subjected to seismic and fire loads. *Fire Saf. J.* 91, 524–531 (2017).
28. EN 1993-1-2 Eurocode 3: Design of steel structures. Part 1–2: General rules—Structural fire design. (2005).
29. Keerthan, P. & Mahendran, M. Numerical studies of gypsum plasterboard panels under standard fire conditions. *Fire Saf. J.* 53, 105–119 (2012).
30. Batista Abreu, J. C., Vieira, L. C. M., Gernay, T. & Schafer, B. W. Cold-formed steel sheathing connections at elevated temperature. *Fire Saf. J.* 123, 103358 (2021).
31. Leng, J., Schafer, B. & Buonopane, S. Modeling the seismic response of cold-formed steel framed buildings: Model development for the CFS-NEES building. in Structural Stability Research Council Annual Stability Conference 426–442 (2013).
32. Zhang, W., Li, Y. & Yu, C. Testing and numerical analysis on cold-formed steel shear walls using corrugated steel sheathing. in Modular and Offsite Construction (MOC) Summit (ed. Al-Hussein, M.) 91–105 (2017). doi:10.29173/mocs56.
33. Ni, S., Yan, X., Hoehler, M. S. & Gernay, T. Numerical Modeling of the Post-Fire Performance of Strap-braced Cold-Formed Steel Shear Wall. *Thin-Walled Struct.* (Under review).
34. Yan, X., Xia, Y., Blum, H. B. & Gernay, T. Post-fire mechanical properties of advanced high-strength cold-formed steel alloys. *Thin-Walled Struct.* 159, 107293 (2021).
35. Ni, S. & Birely, A. C. Post-fire seismic behavior of reinforced concrete structural walls. *Eng. Struct.* 168, (2018).